

Unlock the Potential of Multi-Resonance Experiments




Download the Guide

RF pulse trains



Observing exocrine pancreas metabolism using a novel pancreas perfusion technique in combination with hyperpolarized [1-¹³C]pyruvate

Anna Rushin¹  | Marc A. McLeod¹ | Mukundan Ragavan²  | Matthew E. Merritt¹

¹Department of Biochemistry and Molecular Biology, College of Medicine, University of Florida, Gainesville, Florida, USA

²Department of Structural Biology, St. Jude Children's Research Hospital, Memphis, Tennessee, USA

Correspondence

Matthew E. Merritt, Department of Biochemistry and Molecular Biology, College of Medicine, University of Florida, Gainesville, FL, USA.
Email: matthewmerritt@ufl.edu

Funding information

This work was supported by NIH National Institute of Diabetes and Digestive and Kidney Diseases R01-DK105346, R01-DK132254, and R01-EB032376 to M.E.M. and NIH T32 Predoctoral Fellowship T32-DK108736 to A.R. A portion of this work was performed in the McKnight Brain Institute at the National High Magnetic Field Laboratory's Advanced Magnetic Resonance Imaging and Spectroscopy (AMRIS) Facility, which is supported by the National Science Foundation Cooperative Agreement No. DMR-2128556 and the State of Florida.

Abstract

In a clinical setting, ex vivo perfusions are routinely used to maintain and assess organ viability prior to transplants. Organ perfusions are also a model system to examine metabolic flux while retaining the local physiological structure, with significant success using hyperpolarized (HP) ¹³C NMR in this context. We use a novel exocrine pancreas perfusion technique via the common bile duct to assess acinar cell metabolism with HP [1-¹³C]pyruvate. The exocrine component of the pancreas produces digestive enzymes through the ductal system and is often neglected in research on the pancreas. Real-time production of [1-¹³C]lactate, [1-¹³C]alanine, [1-¹³C]malate, [4-¹³C]malate, [1-¹³C]aspartate, and H¹³CO₃⁻ was detected. The appearance of these resonances indicates flux through both pyruvate dehydrogenase and pyruvate carboxylase. We studied excised pancreata from C57BL/6J mice and NOD. *Rag1*^{-/-}.AI4^{α/β} mice, a commonly used model of Type 1 Diabetes (T1D). Pancreata from the T1D mice displayed increased lactate to alanine ratio without changes in oxygen consumption, signifying increased cytosolic NADH levels. The mass isotopologue analysis of the extracted pancreas tissue using gas chromatography–mass spectrometry revealed confirmatory ¹³C enrichment in multiple TCA cycle metabolites that are products of pyruvate carboxylation. The methodology presented here has the potential to provide insight into mechanisms underlying several pancreatic diseases, such as diabetes, pancreatitis, and pancreatic cancer.

KEYWORDS

¹³C, energy metabolism, hyperpolarized pyruvate, nuclear magnetic resonance, pancreas, perfusion

1 | INTRODUCTION

The pancreas functions as both an endocrine and exocrine gland. The islets of Langerhans form the endocrine component and contain several cell types that produce

hormones. α -Cells produce glucagon, and β -cells produce insulin to regulate glucose metabolism. Simultaneously, acinar cells in the exocrine tissue produce pancreatic enzymes such as amylases and chymotrypsin. These digestive enzymes are released into the pancreatic ductal

system and later deposited into the duodenum. The pancreas is the first organ affected by Type I Diabetes (T1D), an autoimmune disease in which immune cells attack the pancreatic β -cells, resulting in the pancreas producing little to no insulin.

Ex vivo organ perfusions are a vital experimental tool to examine individual organ function. This research model retains the native cellular organization and microstructure of the specific organ while enabling precise control of the nutritional environment. Prior studies have applied the ex vivo perfusion extensively to the liver^{1–4} and heart^{5,6} to examine the metabolic state. Numerous diseases, such as cardiac ischemia, nonalcoholic fatty liver disease, and diabetes, can be characterized by alterations in metabolic substrate selection. The perfused rat heart was used to demonstrate an instantaneous loss of carbohydrate oxidation after ischemia, with profound upregulation of lactate production.^{5,7} Additionally, methods have been developed to explore pyruvate carboxylase activity⁸ as well as flux through the pentose phosphate pathway⁹ and gluconeogenesis.^{3,10} Determining substrate selection in disease states provides insights that can inform development of treatment approaches. For example, suppressing hepatic anaplerotic and cataplerotic flux in a mouse model of obesity was shown to restore regulation of gluconeogenesis and minimize insulin resistance by protecting against rises in oxidative stress.¹

The pancreas has previously been perfused in situ, primarily to investigate local hormonal secretion.^{11,12} In this approach, the pancreas is perfused through the coeliac and the superior mesenteric artery by cannulation of the abdominal aorta. Effluent is collected from the portal vein. The pancreas consists of the endocrine glands, which are commonly known as the islets of Langerhans, and the exocrine tissue, which contains acinar cells. The islets secrete hormones such as insulin and glucagon to regulate blood glucose. The exocrine pancreas synthesizes, stores, and secretes digestive enzymes into the duodenum through the ampulla of Vater. Although the pancreatic islets form only 1%–2% of the pancreatic tissue, they are highly vascularized and receive up to 20% of the total pancreatic blood flow.¹³ During an in situ perfusion, secretagogues are administered to stimulate hormone secretion. This approach has permitted the study of islet hormone secretion within the context of the exocrine pancreatic tissue under various conditions, such as a diabetic state or with pharmacological intervention.¹⁴

A limited number of studies have examined central carbon metabolism in the pancreas. These studies have primarily analyzed metabolism in pancreatic β -cells in vitro as it relates to glucose-stimulated insulin secretion (GSIS).^{15,16} Several metabolic pathways have been associated with GSIS, such as the tricarboxylic acid

(TCA) cycle, glutamine metabolism, reductive TCA cycle flux, and the pentose phosphate pathway.^{15,17} Furthermore, stable isotopes have been utilized to investigate specific metabolic processes in the pancreas. Carbon-13 nuclear magnetic resonance analysis was used to demonstrate a linear relationship between pyruvate cycling and GSIS, whereas pyruvate flux into the TCA cycle through pyruvate dehydrogenase did not correlate with GSIS capacity.¹⁸ Additionally, rates of glucose cycling were recently quantified in the pancreatic islets using [²H₇]glucose.¹⁹ Despite the focus on islet metabolism, studies of metabolic flux in the exocrine pancreas are extraordinarily limited. One study examined oxidation rates of various metabolites in isolated mouse acini by measuring ¹⁴CO₂ production.²⁰ They determined acinar cells preferentially metabolize glutamine over glucose, leucine, and palmitate. Glutamine accumulates in the pancreas and is converted to glutamate for secretion into the duodenum. This is consistent with previous results in rat pancreas slices demonstrating that glutamate formed from leucine typically accumulates intracellularly, whereas the glutamate derived from glutamine is primarily secreted.²¹ Outside of these results, flux through central carbon metabolic pathways is not well understood in the exocrine pancreas.

This work introduces a novel ex vivo pancreas perfusion technique that permits investigation of exocrine metabolism. Here, this perfusion method is combined with NMR and hyperpolarized (HP) substrates. Hyperpolarization²² greatly increases the signal to noise in the collected NMR spectra, thus enabling visualization of metabolic reactions in real time in the perfusing pancreas. In this work, we examined pancreatic metabolism using hyperpolarized [¹⁻¹³C]pyruvate in C57BL/6J mice after perfusion with 3 or 16.7 mM glucose as well as NOD.*Rag1*^{-/-} control mice and NOD.*Rag1*^{-/-}.AI4 ^{α/β} T1D mice after perfusion with 16.7 mM glucose. We detected several central carbon metabolites, such as lactate, alanine, and malate, and further analyzed pool sizes and fractional enrichment profiles of metabolites using gas chromatography–mass spectrometry (GC-MS). Our results indicate that HP pyruvate as a metabolic contrast agent can provide significant insights into pancreatic acinar cell metabolism.

2 | MATERIALS AND METHODS

2.1 | Pancreas perfusions

Pancreas perfusions were performed using male C57BL/6J mice (8–10 weeks old) in the fed state ($n = 8$). Additional experiments were performed using from NOD.*Rag1*^{-/-} control mice ($n = 3$) or NOD.*Rag1*^{-/-}.AI4 ^{α/β}

T1D mice ($n = 4$). The mice were anesthetized using isoflurane followed by euthanasia with cervical dislocation and removal of the heart. The ampulla of Vater was ligated, and the common bile duct was cannulated. The pancreas was excised from the mouse and connected to a glass perfusion column, the entirety of which was inserted into the bore of a 14-T NMR magnet. Perfusion of the pancreas occurred for approximately 30 min at 37°C. The perfusate contained Krebs–Henseleit electrolytes (25 mM NaHCO₃, 112 mM NaCl, 4.7 mM KCl, 1.2 mM each of MgSO₄ and KH₂PO₄, 0.5 mM sodium-EDTA, and 1.25 mM CaCl₂), 1 mM sodium lactate, 0.1 mM sodium pyruvate, and either 3 or 16.7 mM glucose. The perfusate also contained 0.63 mM mixed fatty acids (containing palmitic acid [22.1% of total], palmitoleic acid [5.2%], stearic acid [2.7%], oleic acid [27%], linoleic acid [37.7%], γ -linolenic acid [2.4%], and docosahexaenoic acid [2.8%]) along with 2% (w/v) bovine serum albumin. Additionally, the perfusate contained either 3 mM ($n = 4$) or 16.7 mM glucose ($n = 4$) in experiments with C57BL/6J mice. Perfusions with the T1D mouse model and control were performed with 16.7 mM glucose. Before and during the perfusion, the perfusate was oxygenated with 95% O₂/5% CO₂ mixed gas to maintain the optimal pH and dissolved oxygen levels. Oxygen consumption was measured twice during each perfusion, approximately every 15 min, using the Oxygraph+ (Hansatech Instruments, UK). The rate of perfusate flow through the pancreas was measured at several points during each individual perfusion and typically ranged from 2 to 4 mL/min. After completion of the perfusion, pancreata were freeze-clamped in liquid nitrogen. All animal experiments were conducted in accordance with the University of Florida Institutional Animal Care and Use Committee approved protocol (#202111581).

2.2 | Dynamic nuclear polarization

[1-¹³C]pyruvic acid doped with 15 mM trityl radical (OX063; tris[8-carboxyl-2,2,6,6-tetra-[2-(1-hydroxyethyl)]-benzo-(1,2-d:4,5-d)-bis-(1,3)-dithiole-4-yl]-methyl sodium salt) and 1 mM ProHance was inserted into a HyperSense polarizer. The sample was hyperpolarized with microwave irradiation (94.116 GHz at 100 mW) at \sim 1.3 K until steady-state polarization was achieved (\sim 1.5 h). The frozen sample was dissolved in 4 mL of hot Krebs–Henseleit electrolytes and rapidly transferred to the 14-T NMR magnet. Three milliliters of the dissolved sample was quickly mixed with 5 mL of Krebs–Henseleit electrolytes for a final concentration of 4 mM [1-¹³C]pyruvate and injected into the perfusion column directly above the perfusing pancreas.²³

2.3 | Nuclear magnetic resonance spectroscopy

Spectra of the perfusing pancreata were collected in 10 mm cryoprobe (Bruker Biospin, Billerica, MA, USA) installed in a 14-T magnet with an Avance III NMR console (Bruker Biospin, USA). Shimming was carried out using the ²³Na signal with final linewidths of \sim 17 Hz. ¹³C spectra (spectral width of 300 ppm; 32,768 data points) were recorded using 15° radiofrequency pulses and ¹H decoupling (WALTZ65) during acquisition with a 3-s repetition time. 10 Hz exponential line broadening and baseline correction using a third-order polynomial function were applied to all spectra. The kinetics of individual metabolites were measured using automatic integration in Bruker TopSpin (v4.1.3) across individual spectra followed by total carbon normalization. Summed spectra were processed in MestReNova (v14.2.1), and peak areas of metabolites were obtained by fitting mixed Lorentzian–Gaussian line shapes. The signals were normalized to the total carbon intensity of a sum spectrum of the 60 data points in time where lactate was present. Resonances were assigned using known chemical shifts and previously reported work with hyperpolarized substrates and ex vivo perfusions.^{24,25} Chemical shift assignments were confirmed with [¹H, ¹³C] HSQC and [¹H, ¹³C] HMBC experiments.

2.4 | GC-MS

Perfused pancreas samples were freeze-clamped and stored at -80°C . 100 ± 5 mg of pancreas tissue were transferred to 2.0-mL microcentrifuge tubes. A large homogenization bead was added to each tube along with 1 mL cold acetonitrile/isopropanol/water (3:3:2 v/v/v). Samples were homogenized for five rounds of 20 s each using a bead homogenizer (FastPrep-24, M.P. Biomedicals, Irvine, CA) and were stored on ice for 5 min between each round. Samples were centrifuged at $10,000 \times g$ and 4°C for 45 min. Supernatants were collected and lyophilized overnight (Thermo Fisher Scientific, Waltham, MA, USA). Dried samples were reconstituted in 200 μL of (1:1 v/v) mixture of acetonitrile/water, vortexed, and chilled at -20°C for at least 2 h. The samples were centrifuged again at $10,000 \times g$ and 4°C for 45 min. One hundred and eighty microliters of supernatant was collected, lyophilized overnight, and reconstituted in 100 μL acetonitrile/water (1:1 v/v) mixture. The samples were chilled at -20°C for at least 2 h before centrifugation at $10,000 \times g$ and 4°C for 45 min. The supernatants were collected in separate Eppendorf tubes.

To analyze TCA cycle intermediates, amino acids, and glycolytic end products, 15 μL of each pancreas extract was dried by airstream in V-Vials (CAS

#W986277NG, Wheaton Kimble). Fifty microliters of methoxyamine HCL in pyridine (Thermo Fisher Scientific, Waltham, MA, USA) was added and allowed to react for 90 min at 30°C. Fifty microliters of *N*-tert-butyl-dimethylsilyl-*N*-methyltrifluoroacetamide (MTBSTFA; ProteoSpec MTBSTFA w/1% TBDCMS, Ricca Chemical Company, Arlington, TX, USA) was then combined with each sample and reacted at 70°C for 30 min. Eighty microliters of derivatized sample was transferred to a glass insert (CAS #13-622-207, Thermo Fisher Scientific, Waltham, MA, USA) inside of a 2-mL autosampler glass vial with a 9-mm PTFE screw cap (CAS #60180-595, Thermo Fisher Scientific, Waltham, MA, USA). Eighty microliters of each sample was automatically injected into the gas chromatograph (Trace 1310) and single quadrupole mass spectrometer using the AI/AS 1300 autosampler (Thermo Fisher Scientific, USA). This system utilized a 30-m RTX-5MS Integra column (Crossbond 5% diphenyl/95% dimethylpolysiloxane CAT# 12623-127, Restek, Bellefonte, PA, USA) and 10-m guard column. Each sample was held at 60°C for 3 min after injection. The temperature was increased by 10°C/min up to 325°C, followed by a 5-min bakeout period. The ion source was held at 230°C, and the transfer line to the MS was maintained at 290°C. Xcaliber software (version 4.1) was used to identify and integrate peaks. ICIS peak fitting with an S/N cutoff threshold of 3 and height cutoff at 5.0% of the peak was applied during batch processing. Metabolite concentrations and pool sizes were determined using an 8-point standard curve with a range of 50–2000 ng/sample for each metabolite. Isotopomer network compartment analysis (INCA) software (version 2.1) was used to correct for natural abundance in fractional enrichment calculations.²⁶

2.5 | Statistical analysis

GraphPad Prism 9 software (GraphPad, La Jolla, CA, USA) was used to perform statistical analysis. Statistical significance was established with *p*-values of less than 0.05 using two-way ANOVA with Fisher's LSD post hoc analysis unless otherwise specified. Data were normally distributed as assessed by the Shapiro–Wilk test. A one-way ANOVA with Fisher's LSD post hoc analysis was used to assess statistical significance in lactate/alanine ratios. MetaboAnalyst 5.0 (Xia Lab, McGill University, Ste. Anne de Bellevue, Montreal, QC, Canada, www.metaboanalyst.ca) was used to perform partial least squares-discriminant analysis (PLS-DA) and a one-way ANOVA with Fisher's LSD on metabolite pool sizes.²⁷

3 | RESULTS

Surgical catheterization of the common bile duct in the pancreas is depicted in Figure 1a. This novel technique permits perfusion through the ductal system, with effluent released from microincisions in the distal end of the pancreas after the organ is removed from the animal. Perfusion of the pancreas in this manner allows investigation of exocrine pancreas metabolism. Pancreata from C57BL/6J mice were perfused under conditions of low glucose (3 mM) or high glucose (16.7 mM) for 30 min prior to exposure to hyperpolarized [1 - 13 C]pyruvate. Pancreata from NOD.*Rag1*^{-/-} control mice or NOD.*Rag1*^{-/-}. AI4^{α/β} T1D mice were similarly perfused under the high glucose condition. HP [1 - 13 C]pyruvate was readily utilized by the pancreas. A representative pseudo-2D NMR

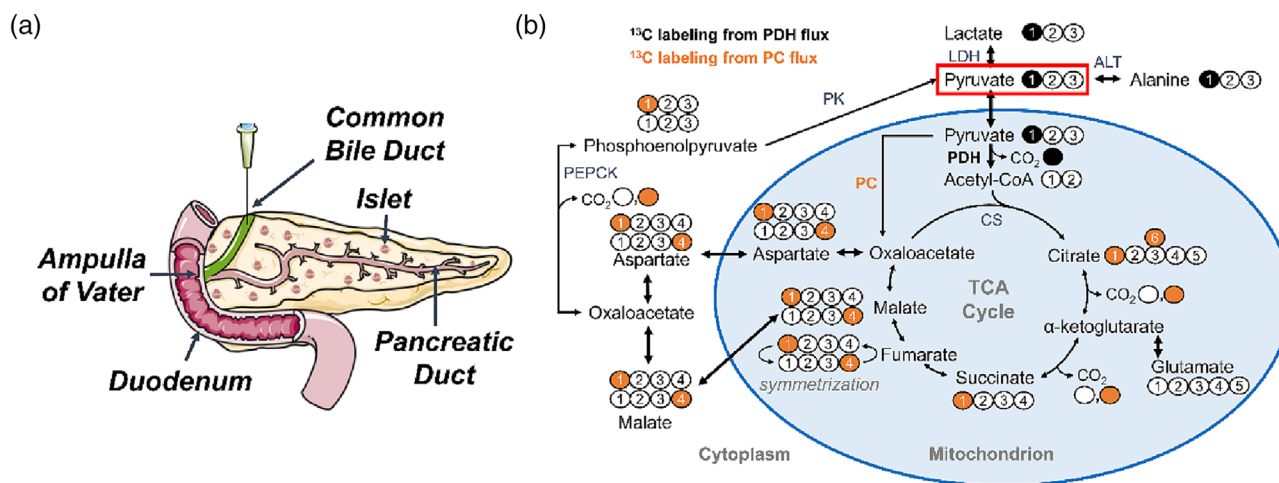


FIGURE 1 (a) Depiction of pancreas anatomy and cannulation of the common bile duct during surgery to initiate exocrine pancreas perfusion. (b) Positional labeling of 13 C in central carbon metabolites resulting from [1 - 13 C]pyruvate.

spectrum displaying the appearance and downstream metabolism of HP [^{13}C]pyruvate is presented in Figure S1. Several metabolites were labeled with ^{13}C , consistent with the predicted positional labeling patterns from the first turn of the TCA cycle (Figure 1b).

Individual hyperpolarized spectra were summed, and a representative spectrum (Figure 2) displays significant pancreatic metabolic activity. In addition to the expected lactate and alanine resonances, signals corresponding to downstream metabolites including malate, aspartate, fumarate, and bicarbonate were observed. Pyruvate carboxylation, via either pyruvate carboxylase or the malic enzyme, is the only source of the four-carbon species observed.

Kinetic curves were generated to visualize the dynamic appearance of [^{13}C]lactate, [^{13}C]alanine, and $\text{H}^{13}\text{CO}_3^-$ in real time after injection of the hyperpolarized [^{13}C]pyruvate (Figure 3). Lactate and alanine were the strongest signals, with alanine emerging concurrently with lactate in some cases. This phenomenon occurred primarily in the C57BL/6J 3 mM group. The appearance of alanine substantially trails that of lactate in the NOD.*Rag1*^{-/-} and the NOD.*Rag1*^{-/-}.AI4^{α/β} groups. Perfusion with 16.7 mM glucose prior to injection of HP [^{13}C]pyruvate increased real-time production of lactate compared to alanine in all groups compared to the C57BL/6J 3 mM group. Pancreata from NOD.*Rag1*^{-/-}.AI4^{α/β} T1D mice displayed similar kinetics to those from the NOD.*Rag1*^{-/-} control mice.

Oxygen consumption in the pancreas was statistically similar between groups (Figure 4a). The normalized signal intensity for each of the downstream metabolites from HP [^{13}C]pyruvate is displayed in Figure 4b,c. HP [^{13}C]lactate was increased in both the NOD.*Rag1*^{-/-} and NOD.*Rag1*^{-/-}.AI4^{α/β} mice compared to the C57BL/6J 3 mM group. The production of HP $\text{H}^{13}\text{CO}_3^-$ and

[^{13}C]fumarate differed between experimental groups. No significant differences were observed between groups for HP [^{13}C]alanine, [^{13}C]aspartate, [^{13}C]malate, or [^{13}C]malate signals. However, the lactate/alanine ratio varied across groups with significant pairwise differences between C57BL/6J mice and both NOD.*Rag1* strains (Figure 4d).

GC-MS was used to assess pool sizes (Figure S2) as well as fractional enrichment of several metabolites in pancreas tissue extracts (Figure 5). The pool sizes of some citric acid cycle intermediates, such as malate and fumarate, increased in the NOD.*Rag1*^{-/-} and NOD.*Rag1*^{-/-}.AI4^{α/β} groups compared to both C57BL/6J groups (Figure S2). The combination of creatine and creatinine, which cannot be distinguished in this analysis, was decreased in the NOD.*Rag1*^{-/-} and NOD.*Rag1*^{-/-}.AI4^{α/β} groups relative to the 16.7 mM C57BL/6J group (Figure S2b,c). Increases in the pool sizes of several amino acids were also found in the NOD.*Rag1*^{-/-}.AI4^{α/β} group compared to both C57BL/6J groups. Additionally, ^{13}C enrichment was detected in various metabolites as shown by fractional enrichment profiles (Figure 5a-k). Notably, the m + 1 mass isotopologue was significantly enriched in lactate and alanine in the 3 mM C57BL/6J group, with further significant increases in the m + 1 mass isotopologue of lactate in the NOD.*Rag1*^{-/-}.AI4^{α/β} group. Additional significant differences were found in the fractional enrichment profiles of several TCA cycle metabolites between the experiment groups.

4 | DISCUSSION

The data demonstrate the observation of central carbon metabolism of the acinar cells that compose the exocrine

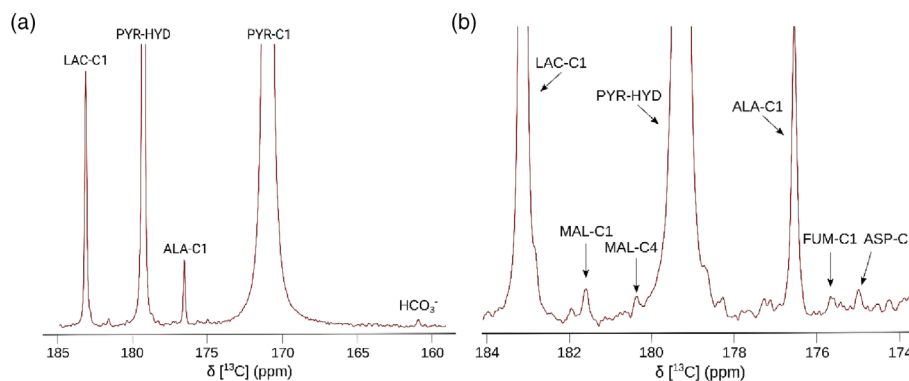


FIGURE 2 Representative ^{13}C NMR spectrum of pancreas metabolic activity after injection with hyperpolarized [^{13}C]pyruvate. Sixty individual spectra beginning from the initial appearance of lactate were summed to generate the displayed representative spectrum. (a) Metabolites with largest peak intensities. (b) Same spectrum as in (a) with intensity scaled to show the metabolites corresponding to smaller peaks. NMR parameters are detailed in the methods section. ALA, alanine; ASP, aspartate; FUM, fumarate; LAC, lactate; MAL, malate; PYR, pyruvate; PYR-HYD, pyruvate hydrate.

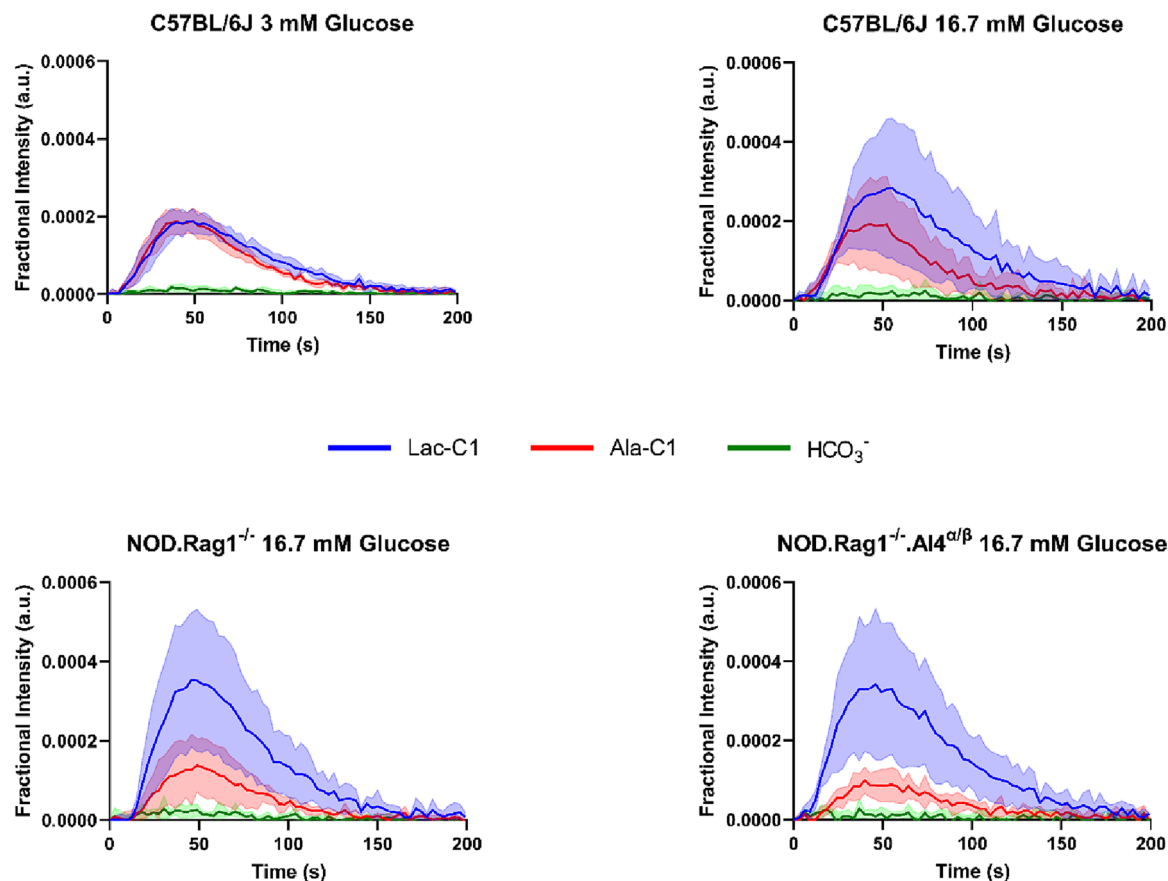


FIGURE 3 Averaged kinetics of lactate, alanine, and HCO_3^- after injection with hyperpolarized $[1-^{13}\text{C}]$ pyruvate in each experimental group over 200 s. Each signal was normalized to total carbon intensity. The shaded area indicates \pm SD for each group. Animals included in each group were C57BL/6J 3 mM ($n = 4$), C57BL/6J 16.7 mM ($n = 4$), NOD.Rag1 $^{-/-}$ ($n = 3$), and NOD.Rag1 $^{-/-}$.AI4 $^{\alpha/\beta}$ ($n = 4$). Two hundred seconds is displayed out of the total data acquisition time of 396 s as this time period best exhibits the appearance and decay of the individual metabolites.

pancreas. The described surgical technique (Figure 1a) has numerous applications in disease research, such as in diabetes, pancreatic cancer, or pancreatitis studies. A model of T1D was explored in this work as the exocrine pancreas is known to exhibit a multitude of abnormalities in T1D that have yet to be explained.²⁸ For example, T1D patients frequently exhibit pancreatic exocrine dysfunction, meaning reduced enzymatic secretions from the exocrine tissue. This usually presents as gastrointestinal symptoms, including abdominal pain and weight loss, and is poorly understood.²⁸ Furthermore, as pancreatitis and pancreatic cancer are primarily diseases of the exocrine tissue,^{29,30} this methodology provides a valuable avenue for future investigation in these fields.

A principal limitation for research in these areas is often a physiologically relevant model.^{31,32} The pancreas perfusion approach presented here permits investigation of pancreatic function while retaining the native structure and secretory function of the whole pancreas. A key advantage of this novel technique is the ability to

examine the exocrine pancreas, whereas the established in situ pancreas perfusion targets the endocrine tissue. The reported experiments were conducted with differing glucose concentrations as almost all of the T1D field focuses on β -cell function. The pancreatic β -cells do not appear to be stimulated using this methodology. This is logical as the islets are not in contact with the pancreatic ductal system and are isolated from the surrounding exocrine tissue by peri-islet basement membranes. Additionally, a lack of compelling metabolic differences between the 3 and 16.7 mM C57BL/6J groups (Figure 4) indicate negligible contributions from the pancreatic islets. Lactate was the most abundant metabolite produced from the pancreas. As the pancreatic β -cells express extraordinarily low levels of lactate dehydrogenase,³³ this denotes the detected signal is predominantly derived from the exocrine tissue.

Hyperpolarized $[1-^{13}\text{C}]$ pyruvate was readily metabolized in the exocrine pancreas. ^{13}C signals corresponding to several downstream metabolites align with expected

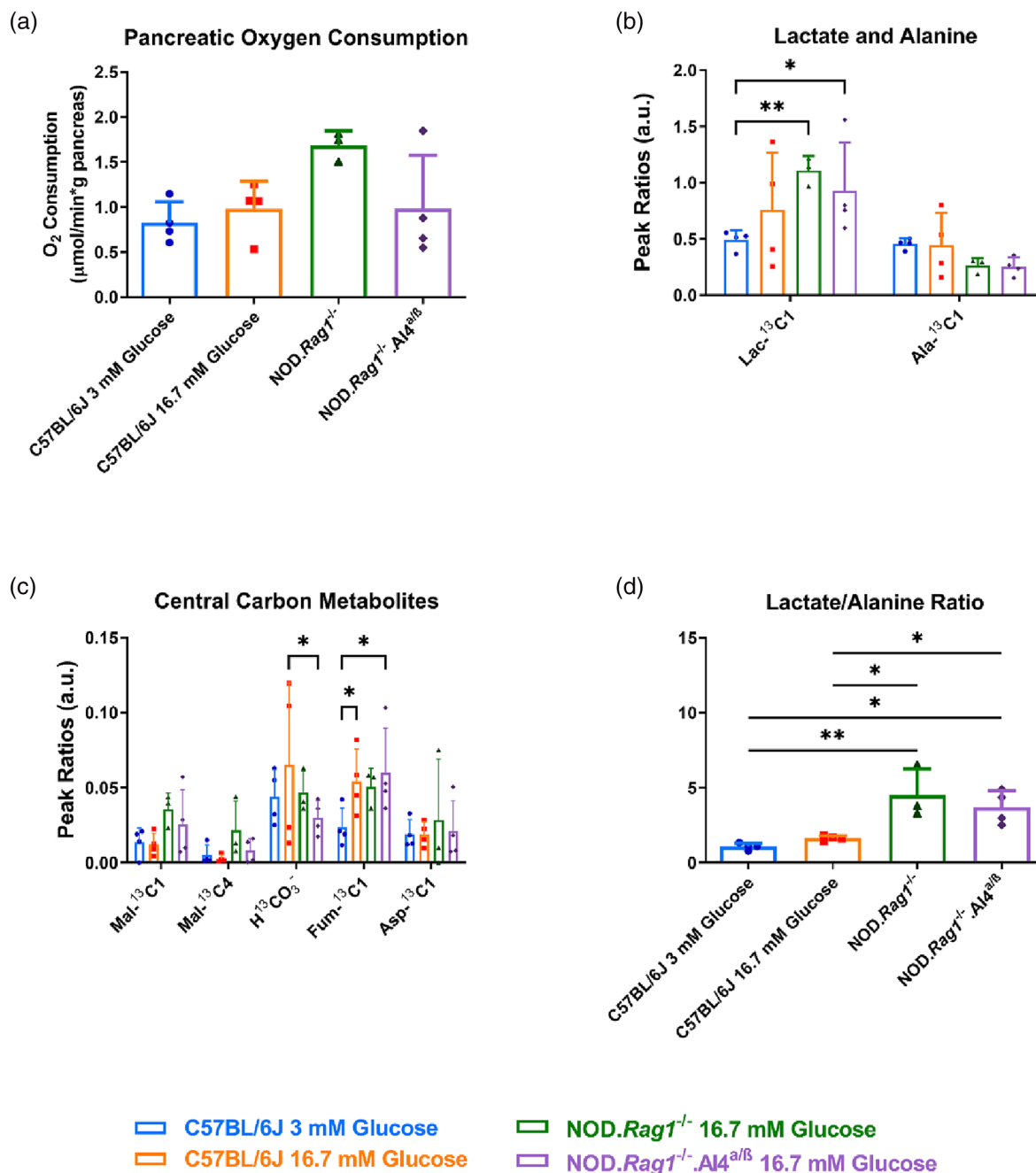


FIGURE 4 (a) Oxygen consumption in the pancreas from C57BL/6J mice during the perfusion with 3 mM ($n = 4$) or 16.7 mM ($n = 4$) unlabeled glucose for 30 min and NOD.Rag1^{-/-} ($n = 3$) and NOD.Rag1^{-/-}.AI4^{α/β} ($n = 4$) mice after perfusion with 16.7 mM unlabeled glucose. (b,c) Ratios of signal intensities of individual resonances detected in summed ¹³C NMR spectra from 60 individual spectra after appearance of [1-¹³C]lactate from the metabolism of hyperpolarized [1-¹³C]pyruvate. Peak ratios were obtained using normalization to the total carbon signal. (d) Ratio of lactate to alanine within each experimental group. ** $p < 0.01$, * $p < 0.05$. Error bars indicate \pm SD. ALA, alanine; ASP, aspartate; FUM, fumarate; LAC, lactate; MAL, malate; PYR, pyruvate; PYR-HYD, pyruvate hydrate.

labeling patterns (Figure 1b) and are depicted in the representative spectra in Figure 2. The dynamic metabolite kinetics display the fast conversion of pyruvate to alanine and lactate. A representative kinetic curve is displayed for each experimental group in Figure 3. Notably, the alanine kinetics shifted between experimental groups. In the

3 mM C57BL/6J group, the alanine appeared at the same time and rate as lactate, a phenomenon that to our knowledge has only occurred in livers lacking PEPCK.^{24,34,35} These data align with knowledge of large pools of alanine in the pancreas,³⁶ which indicates additional physiological roles for alanine, such as promoting

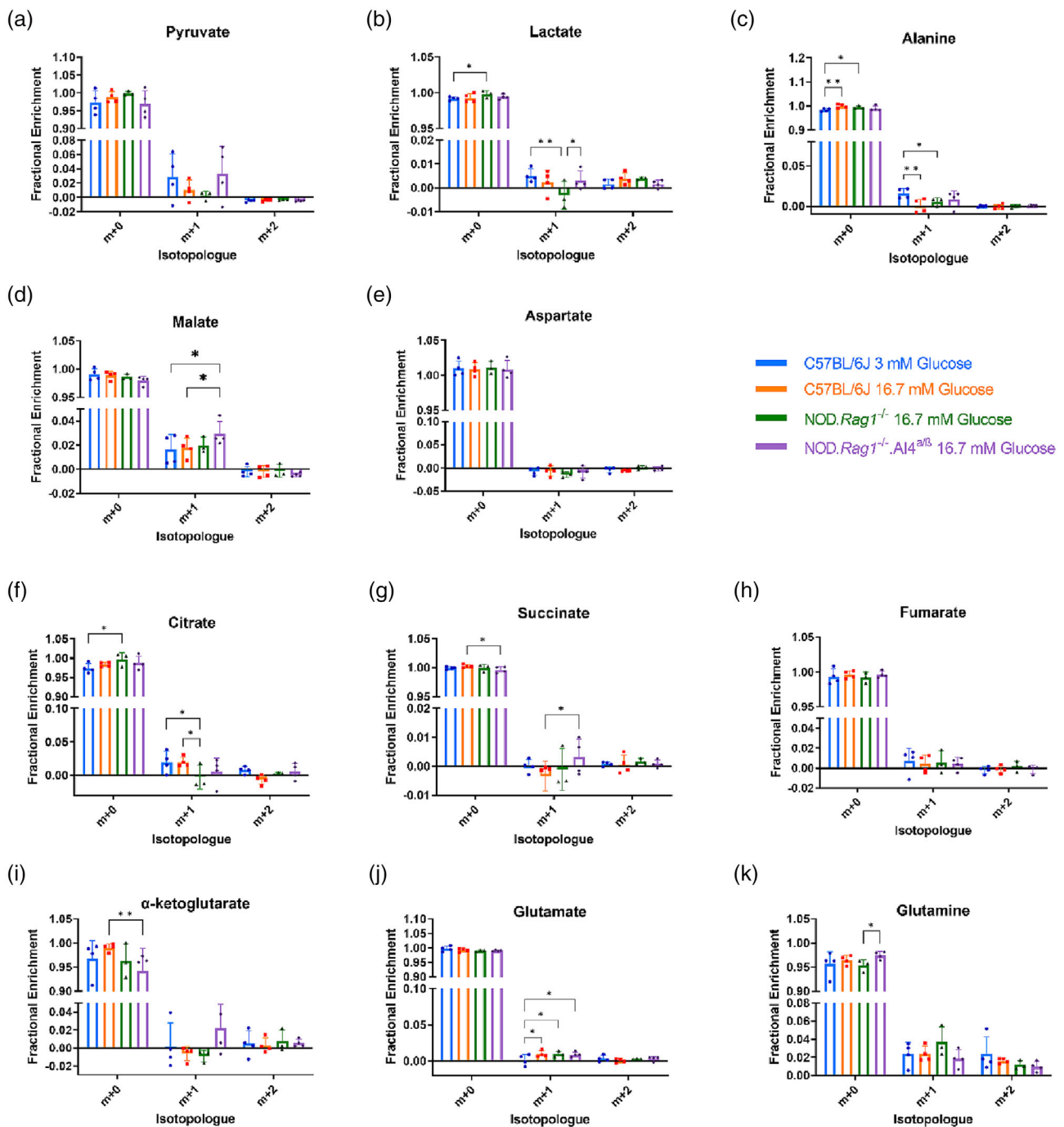


FIGURE 5 Mass isotopologue distributions depicting ^{13}C enrichment of various central carbon metabolites in extracted pancreas tissue after exposure to hyperpolarized $[1-^{13}\text{C}]$ pyruvate. ** $p < 0.01$, * $p < 0.05$. Error bars indicate \pm SD. Animals included in each group were C57BL/6J 3 mM ($n = 4$), C57BL/6J 16.7 mM ($n = 4$), NOD.Rag1^{-/-} ($n = 3$), and NOD.Rag1^{-/-}.AI4 ^{α/β} ($n = 4$).

insulin secretion.³⁷ Relatively large pools of alanine are evident in our GC-MS data as well (Figure S3). However, the appearance of alanine was delayed compared to lactate in the NOD.Rag1^{-/-} and NOD.Rag1^{-/-}.AI4 ^{α/β} experimental groups. This suggests there may be species-dependent differences in the kinetics of pancreatic metabolism. Furthermore, the NOD.Rag1^{-/-}.AI4 ^{α/β} mice displayed increased lactate/alanine (Figure 4), which is

an indicator of elevated NADH:NAD⁺ ratio in the cytosol. A similar shift in this ratio has previously been reported in the diseased pancreas.^{38,39} An ex vivo means of detecting this ratio provides a powerful insight into the cytosolic redox homeostasis.

To further examine pancreatic energetics, pool sizes and ^{13}C fractional enrichment profiles were analyzed in several central carbon metabolites (Figures 5, S2, and S3).

Some citric acid intermediate pool sizes, such as malate, increased in the NOD.*Rag1*^{-/-}.AI4^{α/β} pancreata compared to both C57BL/6J groups (Figure S2b,c). This correlates with increased fractional enrichment in malate m + 1 (Figure 5d) as well as a trend of increased malate C4 peak area in the HP spectra in the NOD.*Rag1*^{-/-}.AI4^{α/β} group compared to the 16.7 mM C57BL/6J group (Figure 4c). The malate-C4 signal only arises after malate-C1 has reacted with fumarase to make fumarate, where the symmetric nature of the fumarate generates malate-C4 after it exchanges through fumarase a second time. HP fumarate-C1(C4) was increased in multiple groups compared to the 3 mM C57BL/6J group (Figure 4c). However, negligible ¹³C enrichment was measured in the extracted tissue (Figure 5h). This suggests the 16.7 mM glucose condition may transiently increase the production of fumarate. Fumarate could be acting as a terminal electron acceptor as previously reported under certain conditions.⁴⁰ However, further studies are needed to fully characterize the role of fumarate in exocrine pancreas metabolism.

Additionally, malate appeared to display a higher level of m + 1 enrichment compared to other TCA cycle metabolites (Figure 5). This could be due to flux through the malic enzyme, which catalyzes the reversible carboxylation of pyruvate to directly form malate, with the resulting consumption of a reducing equivalent in the form of NADPH. Alternatively, the increased enrichment could be due to the enzymatic activity of pyruvate carboxylase, which produces oxaloacetate from pyruvate. These enzymatic pathways are not readily distinguished outside of NMR based saturation experiments, which were not performed here.⁴¹ The occurrence of both pyruvate carboxylation⁴² and pyruvate cycling⁴³ has been demonstrated in pancreatic cells. Furthermore, the isotopic labeling of metabolites decreases as the number of enzymatic steps from the initial labeled substrate increases. This also provides a plausible explanation for the increased enrichment in malate compared to other TCA cycle metabolites.

Increases in several amino acids were also detected; amino acids have been known to affect pancreatic exocrine secretions with varying results. The pool size of creatine was decreased in the NOD.*Rag1*^{-/-} and NOD.*Rag1*^{-/-}.AI4^{α/β} groups, which may be indicative of decreased pancreatic synthesis of creatine⁴⁴ or related to the stimulatory role of creatine in insulin secretion.⁴⁵ As is typical in hyperpolarization experiments due to the short exposure time, ¹³C enrichment was low (0%–5%) in all metabolites.⁴⁶ Clear enrichment of pyruvate, lactate, and alanine m + 1 isotopologues was observed (Figure 5a–c), particularly in the 3 mM C57BL/6J group. The lower glucose availability prior to HP pyruvate

exposure may have decreased metabolic substrate competition in C57BL/6J pancreata exposed to 3 mM glucose, thus leading to higher enrichment. The citrate m + 0 mass isotopologue was significantly lower in the 3 mM C57BL/6J group as well with a corresponding increase in the m + 1 isotopologue (Figure 5f). Citrate is labeled from the precursor pool of OAA, thus suggesting OAA incorporated more of the ¹³C label under the lower glucose condition.

We have demonstrated a platform to investigate exocrine pancreas metabolism by combining a novel surgical technique with HP [¹⁻¹³C]pyruvate and further analysis by GC-MS on the pancreas tissue. Prior to this work, hyperpolarization had not been used to exclusively study the complete pancreas. HP ¹³C imaging provides a noninvasive methodology to assess organ metabolism and is currently under investigation in clinical research settings.^{47–50} This study demonstrated the metabolic kinetics in the pancreas can shift in a species-dependent manner. The NOD.*Rag1*^{-/-}.AI4^{α/β} T1D mouse model displayed increased NADH:NAD⁺ ratio, indicating the cytosolic redox homeostasis may be disrupted in the exocrine pancreas in T1D. Pancreatic metabolism specifically was recently visualized in humans using HP [¹⁻¹³C]pyruvate in whole-abdomen imaging.³⁶ This development establishes immediate clinical relevance to advancing the metabolic understanding in the pancreas, particularly in disease states.

AUTHOR CONTRIBUTIONS

Anna Rushin and Matthew E. Merritt designed the study. Anna Rushin, Marc A. McLeod, and Mukundan Ragavan performed pancreas perfusions. Mukundan Ragavan performed NMR spectroscopy and supervised NMR data collection. Anna Rushin performed GC-MS. Anna Rushin and Matthew E. Merritt analyzed the data and wrote the initial draft. Matthew E. Merritt supervised the study and edited the manuscript. All authors contributed to the article and approved the submitted version.

PEER REVIEW

The peer review history for this article is available at <https://www.webofscience.com/api/gateway/wos/peer-review/10.1002/mrc.5382>.

DATA AVAILABILITY STATEMENT

The raw data associated with this article will be made available by the authors, without undue reservation.

ORCID

Anna Rushin  <https://orcid.org/0000-0002-5643-0101>

Mukundan Ragavan  <https://orcid.org/0000-0001-8678-4229>

REFERENCES

- [1] S. Satapati, B. Kucejova, J. A. G. Duarte, J. A. Fletcher, L. Reynolds, N. E. Sunny, T. He, L. Arya Nair, K. Livingston, X. Fu, M. E. Merritt, A. Dean Sherry, C. R. Malloy, J. M. Shelton, J. Lambert, E. J. Parks, I. Corbin, M. A. Magnuson, J. D. Browning, S. C. Burgess, *J. Clin. Invest.* **2015**, *125*, 4447.
- [2] S. C. Burgess, N. Hausler, M. Merritt, F. M. H. Jeffrey, C. Storey, A. Milde, S. Koshy, J. Lindner, M. A. Magnuson, C. R. Malloy, A. D. Sherry, *J. Biol. Chem.* **2004**, *279*, 48941.
- [3] M. Ragavan, M. A. McLeod, A. Rushin, M. E. Merritt, *Front. Physiol.* **2022**, *13*, 832403. <https://doi.org/10.3389/fphys.2022.832403>
- [4] K. X. Moreno, C. L. Moore, S. C. Burgess, A. D. Sherry, C. R. Malloy, M. E. Merritt, *Metabolomics* **2015**, *11*, 1144.
- [5] A. Akki, K. Smith, A. M. L. Seymour, *Mol. Cell. Biochem.* **2008**, *311*, 215.
- [6] M. Ragavan, A. Kirpich, X. Fu, S. C. Burgess, L. M. McIntyre, M. E. Merritt, *Am. J. Physiol. Heart Circ. Physiol.* **2017**, *312*, 1215.
- [7] M. E. Merritt, C. Harrison, C. Storey, A. D. Sherry, C. R. Malloy, *Magn. Reson. Med.* **2008**, *60*, 1029. <https://doi.org/10.1002/mrm.21760>
- [8] J. Chen, E. P. Hackett, Z. Kovacs, C. R. Malloy, J. M. Park, *Magn. Reson. Med.* **2021**, *85*, 1175.
- [9] K. X. Moreno, C. E. Harrison, M. E. Merritt, Z. Kovacs, C. R. Malloy, A. Dean Sherry, *NMR Biomed.* **2017**, *30*, e3713. <https://doi.org/10.1002/NBM.3713>
- [10] M. Ragavan, M. A. McLeod, A. G. Giacalone, M. E. Merritt, *Metabolites* **2021**, *11*, 441. <https://doi.org/10.3390/METABO11070441/S1>
- [11] V. Leclercq Meyer, J. Marchand, R. Leclercq, W. Malaisse, *Diabetes Metab.* **1976**, *2*, 57.
- [12] A. H. Sparre-Ulrich, L. S. Hansen, B. Svendsen, M. Christensen, F. K. Knop, B. Hartmann, J. J. Holst, M. M. Rosenkilde, *Br. J. Pharmacol.* **2016**, *173*, 27.
- [13] M. Muratore, C. Santos, P. Rorsman, *Comp. Biochem. Physiol. A Mol. Integr. Physiol.* **2021**, *252*, 110846.
- [14] W. H. Li, *Semin. Cell Dev. Biol.* **2020**, *103*, 14.
- [15] M. Huang, J. W. Joseph, *Islets* **2012**, *4*, 210. <https://doi.org/10.4161/isl.20141>
- [16] P. Spégel, L. E. Andersson, P. Storm, V. Sharoyko, I. Göhring, A. H. Rosengren, H. Mulder, *Endocrinology* **2015**, *156*, 1995.
- [17] G. F. Zhang, M. V. Jensen, S. M. Gray, K. El, Y. Wang, D. Lu, T. C. Becker, J. E. Campbell, C. B. Newgard, *Cell Metab.* **2021**, *33*, 804.
- [18] D. Lu, H. Mulder, P. Zhao, S. C. Burgess, M. V. Jensen, S. Kamzolova, C. B. Newgard, A. D. Sherry, *Proc. Nat. Acad. Sci. U.S.A.* **2002**, *99*, 2708.
- [19] M. L. Wall, L. D. Pound, I. Trenary, R. M. O'Brien, J. D. Young, *Diabetes* **2015**, *64*, 2129.
- [20] S. Araya, E. Kuster, D. Gluch, L. Mariotta, C. Lutz, T. V. Reding, R. Graf, F. Verrey, S. M. R. Camargo, *Am. J. Physiol. Gastrointest. Liver Physiol.* **2018**, *314*, G517.
- [21] D. Schachter, J. Buteau, *Am. J. Physiol. Gastrointest. Liver Physiol.* **2014**, *306*, 938.
- [22] J. H. Ardenkjær-Larsen, B. Fridlund, A. Gram, G. Hansson, L. Hansson, M. H. Lerche, R. Servin, M. Thaning, K. Golman, *Proc. Nat. Acad. Sci. U.S.A.* **2003**, *100*, 10158.
- [23] L. Lumata, C. Yang, M. Ragavan, N. Carpenter, R. J. DeBerardinis, M. E. Merritt, *Methods Enzymol.* **2015**, *561*, 73.
- [24] M. E. Merritt, C. Harrison, A. D. Sherry, C. R. Malloy, S. C. Burgess, *Proc. Nat. Acad. Sci. U.S.A.* **2011**, *108*, 19084.
- [25] J. A. M. Bastiaansen, M. E. Merritt, A. Comment, *Sci. Rep.* **2016**, *6*, 1.
- [26] J. D. Young, *Bioinformatics* **2014**, *30*, 1333.
- [27] Z. Pang, J. Chong, G. Zhou, D. A. de Lima Morais, L. Chang, M. Barrette, C. Gauthier, P. É. Jacques, S. Li, J. Xia, *Nucleic Acids Res.* **2021**, *49*, W388.
- [28] M. Campbell-Thompson, T. Rodriguez-Calvo, M. Battaglia, *Curr. Diab. Rep.* **2015**, *15*, 79.
- [29] T. J. Grant, K. Hua, A. Singh, *Prog. Mol. Biol. Transl. Sci.* **2016**, *144*, 241.
- [30] S. N. Duggan, *Proc. Nutr. Soc.* **2017**, *76*, 484.
- [31] D. Osuna de la Peña, S. M. D. Trabulo, E. Collin, Y. Liu, S. Sharma, M. Tatari, D. Behrens, M. Erkan, R. T. Lawlor, A. Scarpa, C. Heeschen, A. Mata, D. Loessner, *Nat. Commun.* **2021**, *12*, 5623. <https://doi.org/10.1038/S41467-021-25921-9>
- [32] S. N. Patel, C. E. Mathews, R. Chandler, C. L. Stabler, *Front. Endocrinol. (Lausanne)* **2022**, *13*, 762.
- [33] N. Sekine, V. Cirulli, R. Regazzi, L. J. Brown, E. Gine, J. Tamarit-Rodriguez, M. Girotti, S. Marie, M. J. MacDonald, C. B. Wollheim, G. A. Rutter, *J. Biol. Chem.* **1994**, *269*, 4895.
- [34] M. E. Merritt, C. Harrison, C. Storey, F. M. Jeffrey, A. D. Sherry, C. R. Malloy, *Proc. Nat. Acad. Sci. U.S.A.* **2007**, *104*, 19773.
- [35] C. Purmal, B. Kucejova, A. Dean Sherry, S. C. Burgess, C. R. Malloy, M. E. Merritt, *Am. J. Physiol. Heart Circ. Physiol.* **2014**, *307*, H1134.
- [36] P. M. Lee, H. Y. Chen, J. W. Gordon, Z. J. Wang, R. Bok, R. Hashoian, Y. Kim, X. Liu, T. Nickles, K. Cheung, F. D. las Alas, H. Daniel, P. E. Z. Larson, C. von Morze, D. B. Vigneron, M. A. Ohliger, *J. Magn. Reson. Imaging* **2022**, *56*, 1792.
- [37] S. J. Parker, C. R. Amendola, K. E. R. Hollinshead, Q. Yu, K. Yamamoto, J. Encarnación-Rosado, R. E. Rose, M. M. LaRue, A. S. W. Sohn, D. E. Biancur, J. A. Paulo, S. P. Gygi, D. R. Jones, H. Wang, M. R. Phillips, D. Bar-Sagi, J. D. Mancias, A. C. Kimmelman, *Cancer Discov.* **2020**, *10*, 1018.
- [38] E. M. Serrao, M. I. Kettunen, T. B. Rodrigues, P. Dzien, A. J. Wright, A. Gopinathan, F. A. Gallagher, D. Y. Lewis, K. K. Frese, J. Almeida, W. J. Howat, D. A. Tuveson, K. M. Brindle, *Gut* **2016**, *65*, 465.
- [39] P. Dutta, S. C. Pando, M. Mascaro, E. Riquelme, M. Zoltan, N. M. Zacharias, S. T. Gammon, D. Piwnicka-Worms, M. D. Pagel, S. Sen, A. Maitra, S. Shams, F. McAllister, P. K. Bhattacharya, *Int. J. Mol. Sci.* **2020**, *21*, 3722. <https://doi.org/10.3390/IJMS21103722>
- [40] J. B. Spinelli, P. C. Rosen, H. G. Sprenger, A. M. Puszynska, J. L. Mann, J. M. Roessler, A. L. Cangelosi, A. Henne, K. J. Condon, T. Zhang, T. Kunchok, C. A. Lewis, N. S. Chandel, D. M. Sabatini, *Science* **2021**, *374*, 1227.
- [41] J. Yang, J. Shen, *J. Magn. Reson.* **2007**, *184*, 344.
- [42] A. N. Lau, Z. Li, L. V. Danai, A. M. Westermark, A. M. Darnell, R. Ferreira, V. Gocheva, S. Sivanand, E. C. Lien, K. M. Sapp, J. R. Mayers, G. Biffi, C. R. Chin, S. M. Davidson, D. A. Tuveson, T. Jacks, N. J. Matheson, O. Yilmaz, M. G. V. Heiden, *Elife* **2020**, *9*, 1.
- [43] M. J. MacDonald, *J. Biol. Chem.* **1995**, *270*, 20051.
- [44] J. B. Walker, *Proc. Soc. Exp. Biol. Med.* **2016**, *98*, 7. <https://doi.org/10.3181/00379727-98-23922>

- [45] B. Ročić, M. V. Lovrenčić, M. Poje, S. J. H. Ashcroft, *Exp. Clin. Endocrinol. Diabetes* **2007**, *115*, 29.
- [46] E. S. Jin, K. X. Moreno, J. X. Wang, L. Fidelino, M. E. Merritt, A. D. Sherry, C. R. Malloy, *NMR Biomed.* **2016**, *29*, 466.
- [47] Z. J. Wang, M. A. Ohliger, P. E. Z. Larson, J. W. Gordon, R. A. Bok, J. Slater, J. E. Villanueva-Meyer, C. P. Hess, J. Kurhanewicz, D. B. Vigneron, *Radiology* **2019**, *291*, 273.
- [48] P. Dutta, T. C. Salzillo, S. Pudakalakatti, S. T. Gammon, B. A. Kaiparettu, F. McAllister, S. Wagner, D. E. Frigo, C. J. Logothetis, N. M. Zacharias, P. K. Bhattacharya, *Cell* **2019**, *8*, 340. <https://doi.org/10.3390/CELLS8040340>
- [49] V. Z. Miloushev, K. L. Granlund, R. Boltyanskiy, S. K. Lyashchenko, L. M. DeAngelis, I. K. Mellinshoff, C. W. Brennan, V. Tabar, T. J. Yang, A. I. Holodny, R. E. Sosa, Y. W. W. Guo, A. P. Chen, J. Tropp, F. Robb, K. R. Keshari, *Cancer Res.* **2018**, *78*, 3755.
- [50] E. M. Serrao, K. M. Brindle, *Front. Oncol.* **2016**, *6*, 59. <https://doi.org/10.3389/FONC.2016.00059>

SUPPORTING INFORMATION

Additional supporting information can be found online in the Supporting Information section at the end of this article.

How to cite this article: A. Rushin, M. A. McLeod, M. Ragavan, M. E. Merritt, *Magn Reson Chem* **2023**, *61*(12), 748. <https://doi.org/10.1002/mrc.5382>